

ANALYSIS OF 2-D THIN STRUCTURES BY THE MESHLESS REGULAR HYBRID BOUNDARY NODE METHOD*

Zhang Jianming Yao Zhenhan

(*Department of Engineering Mechanics, Tsinghua University, Beijing 100084, China*)

ABSTRACT Thin structures are generally solved by the Finite Element Method (FEM), using plate or shell finite elements which have many limitations in applications, such as numerical locking, edge effects, length scaling and the convergence problem. Recently, by proposing a new approach to treating the nearly-singular integrals, Liu et al. developed a BEM to successfully solve thin structures with the thickness-to-length ratios in the micro- or nano-scales. On the other hand, the meshless Regular Hybrid Boundary Node Method (RHBNM), which is proposed by the current authors and based on a modified functional and the Moving Least-Square (MLS) approximation, has very promising applications for engineering problems owing to its meshless nature and dimension-reduction advantage, and not involving any singular or nearly-singular integrals. Test examples show that the RHBNM can also be applied readily to thin structures with high accuracy without any modification.

KEY WORDS shell-like structures, meshless, moving least squares approximation, hybrid boundary node method

I . INTRODUCTION

The Finite Element Method (FEM) has been a successful tool for the analysis of plate and shell structures in engineering using plate and shell elements. The plate and shell elements are based on plate and shell theories in which many assumptions about the geometry, loading and deformation of structure are introduced when a 3-D body is abstracted into a 2-D model. Therefore, various pitfalls are also introduced, such as numerical locking, edge effect, length scaling and especially the convergence problem (the FEM may not converge or converge to wrong answers under certain conditions^[1]), restricting the application of the FEM in many ways. For example, when a plate is linked to a block body in a structure, different elements have to be used and special techniques are required to deal with the linkage, resulting in lower accuracy (especially for the stresses) at or near the linkage than elsewhere, while the stresses at the linkage are of greater concern to engineers. Furthermore, it is often difficult for structure analyzing engineers to distinguish among thin shell, thick shell and blocks, to choose the right type of finite elements accordingly in the analysis of a complicated structure. In view of above fact, it is desirable to turn to the 3-D elasticity theory in building numerical models for plate- and shell-like structures, which have nonuniform thicknesses or are linked to bulky solids, in a unified formulation. Unfortunately, this has not been achieved in the FEM using the plate and shell theories, although a great deal of research effort has been made in the last three decades.

* Received 4 April 2001; revision received 26 October 2001.

The Boundary Element Method (BEM) has been regarded as unsuitable for dealing with thin structures for quite some time. Recently, Liut et al.^[2,3] have proved theoretically and verified numerically that the BEM does not degenerate when it is applied to a thin shell-like structure, contrary to the case of crack-like problems. By proposing a new approach of treating nearly-singular integrals, they successfully developed the BEM to solve thin structures with the thickness-to-length ratios in the micro- or nano-scales^[2,3].

Meshless methods have been gaining popularity ever since the publication of the element free Galerkin (EFG) method by Belytschko et al.^[4], in which although no mesh is required for the interpolation of the solution variables, background cells are inevitable for the integration of ‘energy’. In 1998, two meshless methods, the Meshless Local Boundary Integral Equation (MLBIE) method by Zhu et al.^[5] and the Meshless Local Petrov-Galerkin (MLPG) approach by Atluri et al.^[6] were developed. Both methods use local weak forms over a local sub-domain and shape functions from the MLS approximation, and lead to truly meshless ones.

In 1997, Mukherjee et al.^[7] proposed a Boundary Node Method (BNM), which combines the MLS with Boundary Integral Equations (BIE). This method is not a truly meshless one yet, as an underlying cell structure is again used for numerical integration.

To combine the advantages of the MLBIE and the BNM, a Hybrid Boundary Node Method (Hybrid BNM) was introduced by Zhang et al.^[8], based on the MLS interpolation scheme and the hybrid displacement variational formulation. This method is a truly meshless one as the MLBIE and MLPG—absolutely no cells are required either for interpolation of the solution variables or for the numerical integration, and has the dimensionality advantage of the BIE or BNM—only scattered nodes are constructed on the boundary of the domain. However, the HBNM has the drawback of “boundary layer effect”, i. e. the accuracy of results in the vicinity of the boundary is very sensitive to the proximity of the interior points to the boundary. To avoid this pitfall, a new meshless Regular Hybrid Boundary Node Method (RHBNM)^[9,10] has been proposed, in which the source points of the fundamental solutions are located outside the domain rather than at the boundary nodes as in the Hybrid BNM or other hybrid boundary element models.

As the RHBNM does not involve any singular or nearly-singular integration, it is possibly viable for thin structures. In this paper, several test examples are presented to demonstrate the effectiveness and high accuracy of the RHBNM in the analysis of the very thin and/or layered structures, which are even in the micro- or nano-scales, as in Refs.^[2,3].

II . THE MLS APPROXIMATION SCHEME FOR THE 2-D RHBNM

This section gives a brief summary of the MLS approximation, whose excellent illustrations can be found in Ref.^[11].

It should be noted that this MLS interpolation scheme will be coupled later with 2-D hybrid displacement variational formulation which uses three independent variables, i. e. displacement u_i in the domain, displacement \tilde{u}_i and traction \tilde{t}_i , $i = 1, 2$, on the boundary, of which the \tilde{u}_i and \tilde{t}_i will be interpolated by MLS scheme. The discussion below use the variables \tilde{u} and \tilde{t} to represent any particular component of the displacement and traction respectively, for the sake of brevity of index notation.

In contrast to the BNM, the MLS interpolation in the present approach is independently performed on piecewise smooth segments Γ_i , $i = 1, 2, \dots, n$ which constitute the boundary naturally rather than on the whole boundary Γ . To approximate the functions \tilde{u} and \tilde{t} on each Γ_i over which a number of

nodes $\{s_I\}$, $I = 1, 2, \dots, N$, are randomly located, the MLS interpolants for \bar{u} and \bar{t} are defined as

$$\bar{u}(s) = \sum_{j=1}^m p_j(s) a_j(s) = \mathbf{p}^T(s) \mathbf{a}(s) \tag{1}$$

$$\bar{t}(s) = \sum_{j=1}^m p_j(s) b_j(s) = \mathbf{p}^T(s) \mathbf{b}(s) \tag{2}$$

where s is a curvilinear co-ordinate on Γ_i , $p_1 = 1$ and $p_j(s)$, $j = 2, \dots, m$ are monomials in s . In this paper, a quadratic background basis is used, i. e.

$$\mathbf{p}^T(s) = [1, s, s^2], \quad m = 3 \tag{3}$$

The coefficient vectors $\mathbf{a}(s)$ and $\mathbf{b}(s)$ are determined by minimizing a weighted discrete L_2 norm, defined as

$$J_1(s) = \sum_{I=1}^N w_I(s) [\mathbf{p}^T(s_I) \mathbf{a}(s) - \hat{u}_I]^2 \tag{4}$$

$$J_2(s) = \sum_{I=1}^N w_I(s) [\mathbf{p}^T(s_I) \mathbf{b}(s) - \hat{t}_I]^2 \tag{5}$$

where points s_I are boundary nodes on Γ_i ; s is the coordinate of an evaluation point E on Γ_i ; N is the number of boundary nodes in the neighborhood of E for which the weight functions $w(s - s_I) > 0$; \hat{u}_I and \hat{t}_I are approximations to the nodal values $u(s_I)$ and $t(s_I)$, respectively.

Solving $\mathbf{a}(s)$ and $\mathbf{b}(s)$ by minimizing J_1 and J_2 in Eqs. (4) and (5), and substituting them into Eqs. (1) and (2) gives a relation which may be written in the form of an interpolation function similar to that used in the FEM, i. e.

$$\bar{u}(s) = \sum_{I=1}^N \Phi_I(s) \hat{u}_I, \quad \bar{t}(s) = \sum_{I=1}^N \Phi_I(s) \hat{t}_I \tag{6,7}$$

where

$$\Phi_I(s) = \sum_{j=1}^m p_j(s) [\mathbf{A}^{-1}(s) \mathbf{B}(s)]_{jI} \tag{8}$$

with the matrices $\mathbf{A}(s)$ and $\mathbf{B}(s)$ defined by

$$\mathbf{A}(s) = \sum_{I=1}^N w_I(s) \mathbf{p}(s_I) \mathbf{p}^T(s_I) \tag{9}$$

$$\mathbf{B}(s) = [w_1(s) \mathbf{p}(s_1), w_2(s) \mathbf{p}(s_2), \dots, w_N(s) \mathbf{p}(s_N)] \tag{10}$$

The MLS approximation is well defined only when the matrix \mathbf{A} in Eq. (9) is non-singular.

Several kinds of weight function can be seen in the literature, the choice of weight functions and the consequences of a choice in the EFG method are discussed in some detail elsewhere^[11]. Gaussian weight function corresponding to node s_I may be written as

$$w_I(s) = \begin{cases} \frac{\exp[-(d_I/c_I)^2] - \exp[-(\hat{d}_I/c_I)^2]}{1 - \exp[-(\hat{d}_I/c_I)^2]}, & 0 \leq d_I \leq \hat{d}_I \\ 0, & d_I \geq \hat{d}_I \end{cases} \tag{11}$$

where $d_I = |s - s_I|$, the absolute value of the distance between an evaluation point and a node, measured along Γ_i , c_I is a constant controlling the shape of the weight function, and \hat{d}_I is the size of the support for the weight function w_I and determines the support of node s_I . The \hat{d}_I should be chosen such that \hat{d}_I would be large enough to have a sufficient number of nodes covered in the domain of definition of every sample point ($N \geq m$) to ensure the regularity of \mathbf{A} .

III . DEVELOPMENT OF THE REGULAR HYBRID BOUNDARY NODE METHOD

In this section, the following 2-D linear elasticity problem is considered

$$\begin{aligned} \sigma_{ij,j} + b_j &= 0, & \forall x \in \Omega \\ u_i &= \bar{u}_i, & \forall x \in \Gamma_u \\ t_i \equiv \sigma_{ij}n_j &= \bar{t}_i, & \forall x \in \Gamma_t \end{aligned} \tag{12}$$

where the domain Ω is enclosed by $\Gamma = \Gamma_u + \Gamma_t$; \bar{u}_i and \bar{t}_i are the prescribed displacement and traction, respectively, on the essential boundary Γ_u and on the traction boundary Γ_t ; and n is the outward normal direction to the boundary Γ , with n_i components.

The hybrid boundary model here proposed is based on a modified variational principle. The functions to be independent are:

- displacement field in the domain, \mathbf{u} , with u_i components;
- boundary displacement field, $\bar{\mathbf{u}}$, with \bar{u}_i components;
- boundary tractions, $\bar{\mathbf{t}}$, with \bar{t}_i components.

The corresponding variational functional, Π_{HB} , is defined as in the hybrid BEM model by De-Figueroa and Brebbia^[12]

$$\Pi_{AB} = \int_{\Omega} \left(\frac{1}{2} u_{i,j} C_{ijkl} u_{k,l} - b_i u_i \right) d\Omega - \int_{\Gamma} \bar{t}_i (u_i - \bar{u}_i) d\Gamma - \int_{\Gamma_t} \bar{t}_i \bar{u}_i d\Gamma \tag{13}$$

In the above equation, the boundary displacement \bar{u}_i satisfies the essential boundary conditions, i.e., $\bar{u}_i = \bar{u}_i$ on Γ_u ; $C_{ijkl} = \frac{2G\nu}{1-2\nu} \delta_{ij} \delta_{kl} + G\delta_{ij} \delta_{kl}$, where G and ν are the shear modulus and Poisson's ratio respectively.

By performing the variation it can be shown that

$$\begin{aligned} \delta\Pi_{AB} &= \int_{\Omega} (-\sigma_{ij,j} - b_i) \delta u_i d\Omega + \int_{\Gamma} (t_i - \bar{t}_i) \delta u_i d\Gamma - \\ &\int_{\Gamma} (u_i - \bar{u}_i) \delta \bar{t}_i d\Gamma - \int_{\Gamma_t} (\bar{t}_i - \bar{t}_i) \delta \bar{u}_i d\Gamma \end{aligned} \tag{14}$$

where σ_{ij} and t_i are the stress tensor and the traction vector, respectively, which are functions of the displacement u_i in the domain.

With the vanishing of $\delta\Pi_{AB}$, the following equivalent integral equations can be obtained

$$\int_{\Gamma} (t_i - \bar{t}_i) \delta u_i d\Gamma - \int_{\Omega} (\sigma_{ij,j} + b_j) \delta u_i d\Omega = 0 \tag{15}$$

$$\int_{\Gamma} (u_i - \bar{u}_i) \delta \bar{t}_i d\Gamma = 0 \tag{16}$$

It can be seen that Eqs. (15) and (16) hold in any sub-domain, for example, in a sub-domain Ω_s and its boundaries Γ_s and L_s (where Ω_s is the intersection of the domain Ω and a circle centered at a boundary node s_j , see Fig.1). Therefore, one can use the following weak forms on the sub-domain to replace Eqs. (15) and (16)

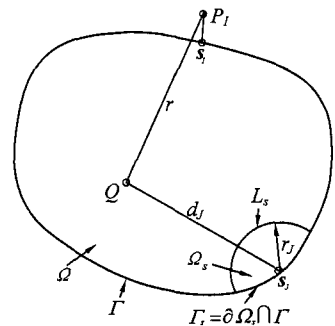


Fig.1 The local domain centered at a node s_j and the source point of fundamental solution corresponding to a node s_i .

$$\int_{\Gamma_s+L_s} (t_i - \bar{t}_i) v d\Gamma - \int_{\Omega} (\sigma_{ij,j} + b_i) v d\Omega = 0 \tag{17}$$

$$\int_{\Gamma_s+L_s} (u_i - \bar{u}_i) v d\Gamma = 0 \tag{18}$$

where v is a test function.

In Eqs. (17) and (18), \bar{u}_i and \bar{t}_i on Γ_s are represented by Eqs. (6) and (7), but \bar{u}_i and \bar{t}_i on L_s have not been defined yet. To solve this problem, we deliberately select v such that all integrals over L_s vanish. This can be easily accomplished by using the weight function in the MLS approximation as v , with the radius \hat{d}_l of the support of the weight function replaced by the radius r_j of the sub-domain Ω_s . For example, for a node s_j

$$v_j(Q) = \begin{cases} \frac{\exp[-(d_j/c_j)^2] - \exp[-(r_j/c_j)^2]}{1 - \exp[-(r_j/c_j)^2]}, & 0 \leq d_j \leq r_j \\ 0, & d_j \geq r_j \end{cases} \tag{19}$$

where d_j is the distance between point Q , in domain Ω , and the nodal point s_j . Therefore, $v_j(Q)$ vanishes on L_s .

As in Ref. [12], the u and t inside Ω and on Γ are defined as

$$u = \begin{Bmatrix} u_1 \\ u_2 \end{Bmatrix} = \sum_{l=1}^{NN} \begin{bmatrix} u'_{l1} & u'_{l2} \\ u'_{l21} & u'_{l22} \end{bmatrix} \begin{Bmatrix} x'_1 \\ x'_2 \end{Bmatrix}, \quad t = \begin{Bmatrix} t_1 \\ t_2 \end{Bmatrix} = \sum_{l=1}^{NN} \begin{bmatrix} t'_{l1} & t'_{l2} \\ t'_{l21} & t'_{l22} \end{bmatrix} \begin{Bmatrix} x'_1 \\ x'_2 \end{Bmatrix} \tag{20,21}$$

where u'_i and t'_i are fundamental solutions with the source point at point P_l , which is located outside the domain and corresponds to node s_j ; x'_i unknown parameters; NN the total number of boundary nodes.

For a 2-D elasticity problem, the fundamental solutions are

$$\begin{aligned} u'_{ij} &= \frac{-1}{8\pi(1-\nu)G} [(3-4\nu)\delta_{ij}\ln(r) - r_{,i}r_{,j}] \\ t'_{ij} &= \frac{-1}{4\pi(1-\nu)r} \left\{ [(1-2\nu)\delta_{ij} + 2r_{,i}r_{,j}] \frac{\partial r}{\partial n} + (1-2\nu)(r_{,i}n_j - r_{,j}n_i) \right\} \end{aligned} \tag{22}$$

where $r(P_l, Q) = \sqrt{[x(Q) - x(P_l)]^2 + [y(Q) - y(P_l)]^2}$; Q and P_l are field point and source point respectively. And P_l is determined by

$$P_l = s_l + h\xi n(s_l) \tag{23}$$

where h is the mesh size; $n(s_l)$ is the outward normal direction to the boundary at node s_l ; and ξ is the scale factor. As can be imagined, the scale factor ξ plays an important role in the performance of the present method. Too small a value for ξ will lead to nearly-singular integrals and thus inaccurate results; On the other hand, too large a one will lead to an ill-posed system of algebraic equations as well. Numerical tests show that the proper range for ξ is between 3.0 and 7.0.

As u is expressed by Eq. (20), the term $\sigma_{ij,j}$ on the left-hand side in Eq. (17) vanishes. By substituting Eqs. (6), (7), (19), (20) and (21) into Eqs. (17) and (18), and omitting the vanished terms and the body force, one has

$$\begin{aligned} \sum_{l=1}^{NN} \int_{\Gamma_s} \begin{bmatrix} u'_{l1} & u'_{l2} \\ u'_{l21} & u'_{l22} \end{bmatrix} \begin{Bmatrix} x'_1 \\ x'_2 \end{Bmatrix} v_j(Q) d\Gamma &= \sum_{l=1}^{NN} \int_{\Gamma_s} \begin{bmatrix} \Phi_l(s) & 0 \\ 0 & \Phi_l(s) \end{bmatrix} \begin{Bmatrix} \hat{u}'_1 \\ \hat{u}'_2 \end{Bmatrix} v_j(Q) d\Gamma \\ \sum_{l=1}^{NN} \int_{\Gamma_s} \begin{bmatrix} t'_{l1} & t'_{l2} \\ t'_{l21} & t'_{l22} \end{bmatrix} \begin{Bmatrix} x'_1 \\ x'_2 \end{Bmatrix} v_j(Q) d\Gamma &= \sum_{l=1}^{NN} \int_{\Gamma_s} \begin{bmatrix} \Phi_l(s) & 0 \\ 0 & \Phi_l(s) \end{bmatrix} \begin{Bmatrix} \hat{t}'_1 \\ \hat{t}'_2 \end{Bmatrix} v_j(Q) d\Gamma \end{aligned} \tag{24}$$

Using the above equations for all nodes, one can obtain the final system of equations

$$\mathbf{U}\mathbf{x} = \mathbf{H}\hat{\mathbf{u}}, \quad \mathbf{T}\mathbf{x} = \mathbf{H}\hat{\mathbf{t}} \quad (25, 26)$$

where

$$\begin{aligned} U_{IJ} &= \int_{\Gamma_s^J} \begin{bmatrix} u'_{11} & u'_{12} \\ u'_{21} & u'_{22} \end{bmatrix} v_J(\mathbf{Q}) d\Gamma, & T_{IJ} &= \int_{\Gamma_s^J} \begin{bmatrix} t'_{11} & t'_{12} \\ t'_{21} & t'_{22} \end{bmatrix} v_J(\mathbf{Q}) d\Gamma \\ H_{IJ} &= \int_{\Gamma_s^J} \begin{bmatrix} \Phi_I(s) & 0 \\ 0 & \Phi_I(s) \end{bmatrix} v_J(\mathbf{Q}) d\Gamma, & \mathbf{x}^T &= [x_1^1, x_2^1, \dots, x_1^N, x_2^N] \\ \hat{\mathbf{t}}^T &= [\hat{t}_1^1, \hat{t}_2^1, \dots, \hat{t}_1^N, \hat{t}_2^N], & \hat{\mathbf{u}}^T &= [\hat{u}_1^1, \hat{u}_2^1, \dots, \hat{u}_1^N, \hat{u}_2^N] \end{aligned}$$

For a well-posed problem, the values of either u_i or t_i are known at each node on the boundary, thus \hat{u}_i^J on Γ_u and \hat{t}_i^J on Γ_t can be obtained by the following equations

$$\hat{u}_i^J = \sum_{J=1}^N R_{IJ} \bar{u}_i^J = \sum_{J=1}^N R_{IJ} \bar{u}_i^J \quad (27)$$

For edges, u_i are prescribed, and

$$\hat{t}_i^J = \sum_{J=1}^N R_{IJ} \bar{t}_i^J = \sum_{J=1}^N R_{IJ} \bar{t}_i^J \quad (28)$$

For edges, t_i are prescribed, where $R_{IJ} = [\Phi_J(s_I)]^{-1}$ and N is the number of nodes on the edge. Therefore, by rearranging the governing Eqs.(25) and (26), one obtains the final system in terms of \mathbf{x} only, and the unknown vector \mathbf{x} is obtained by solving the final equation system. Displacements u_i and tractions t_i at any point inside domain Ω or on the boundary Γ are evaluated by Eqs.(20) and (21) without further integration.

From the above discussion, one can see that the present method is not merely a truly meshless one, but also a regular one, as no singular integrals or nearly-singular integrals are involved. So it may be used to solve thin shell-like structure problems.

IV. NUMERICAL VERIFICATIONS

To verify the RHBNM for thin structure problems, three test examples are studied in this section, together with comparisons with exact solutions (where available). In all examples, the size of support for weight function, \hat{d}_J in Eq.(11), is taken to be $9.0h$, with h as the mesh size, and the parameter c_J is taken to be such that \hat{d}_J/c_J is constant and equal to 4.0. The size of the local domain (radius r_J) for each node is chosen as $1.0h$ in all computations and the parameter c_J in Eq.(19) is taken to be such that r_J/c_J is constant and equal to 4.0. The scale factor ξ in Eq.(23) for the first example is taken to be 7.0 and for the next two examples, 3.0. Also, in all integrations, 5 Gauss points are used on each of the two half-parts of Γ_s .

4.1 Test Problem 1: Displacement Field Problem on an Ellipse

The geometry of this problem is shown in Fig.2. The half-length of the major axis a is kept constant in the study, while the half-length of the minor axis b varies from $1.0a$ to $1.0 \times 10^{-6}a$. This setup, therefore, provides a model of the ellipse which can be categorized as a thin shell, a thick shell and even a bulky solid, depending on the values of the ratio b/a .

A planar displacement profile is described on the boundary as follows

$$u_1 = y^3 - 3yx^2, \quad u_2 = -x^3 + 3xy^2$$

40 nodes, uniformly placed, are used on the boundary. The output is the relative error defined by a L_2 norm as

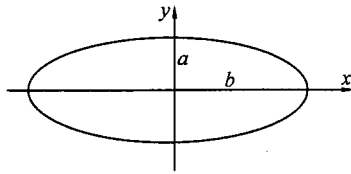


Fig.2 Displacement field problem on an ellipse.

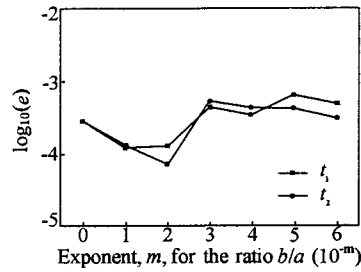


Fig.3 Relative errors of tractions \$t_1\$ and \$t_2\$ along the boundary.

$$e = \frac{1}{|t|_{\max}} \sqrt{\frac{1}{N} \sum_{i=1}^N (t_i^{(e)} - t_i^{(n)})^2}$$

where \$|t|_{\max}\$ is the maximum value of \$t\$ over \$N\$ sample points, the superscripts \$(e)\$ and \$(n)\$ refer to the exact and numerical solutions, respectively. Plane strain cases with Young's modulus \$E = 2.5\$ (in consistent units) and the Poisson's ratio \$\nu = 0.3\$ have been considered for various ratios \$b/a\$. The relative errors of tractions \$t_1\$ and \$t_2\$ along the whole boundary (with 44 uniformly spaced sample points) are shown in Fig.3. It can be seen that the accuracy of the present RHBNM remains very high even for the ratio \$b/a\$ in the micro-scale. It should be pointed out that this problem, when the ratio \$b/a\$ is in the micro-scale, cannot be solved by the BIE/BEM owing to the displacement boundary conditions, as discussed in Ref. [2].

4.2 Test Problem 2: Thin Coating on a Shaft

To compare with the BEM developed by Liu et al^[3], the next two related test examples of a shaft with a thin coating are taken from Ref. [3], in which the calculation of conventional BEM and FEM for these problems and a comparison of the results by these methods are given.

The geometry of the shaft and coating is shown in Fig.4. The shaft and coating have outer radii \$r_s\$ and \$r_c\$ respectively, which are considered here: (a) the thickness \$h = r_c - r_s\$ of the coating is uniform and approaches zero while \$r_s\$ remains constant, as shown in Fig.4(a), and (b) the coating is of non-uniform thickness; both \$r_s\$ and \$r_c\$ remain constant, but their centers are misaligned, producing some normalized eccentricity \$\delta = \frac{x_c}{r_c - r_s}\$, where \$x_c\$ is the center offset, as shown in Fig.4(b). In both cases, uniform pressure \$p\$ acts on the outer circumference of the coating, and essential boundary conditions, \$u_1 = u_2 = 0\$, are prescribed around the inner circumference. Plane strain conditions with Young's modulus \$E = 1.92 \times 10^9\$ Pa and the Poisson's ratio \$\nu = 0.2\$ are assumed and 40 uniformly spaced nodes are used, 20 on the outer circle and 20 the inner circle.

For the case (a), an analytical solution for the stress field can be obtained. The relative error of the radial stress \$\sigma_r\$ at point A, defined as % error = \$\left| \frac{\sigma_{\text{Exact}} - \sigma_{\text{RHBNM}}}{\sigma_{\text{Exact}}} \right| \times 100\$, is shown in Fig.5 while the coating thickness varies in the range of \$10^{-1} r_s - 10^{-10} r_s\$. Note that as the coating thickness decreases, the solution accuracy remains stable and is very high.

Figure 6 shows the normalized radial stress \$\sigma_r\$ at point A. Note that the asymptotic behavior of the RHBNM solution approaches the analytical value of the sample problem as \$\delta \to 0\$ (case (a)), and

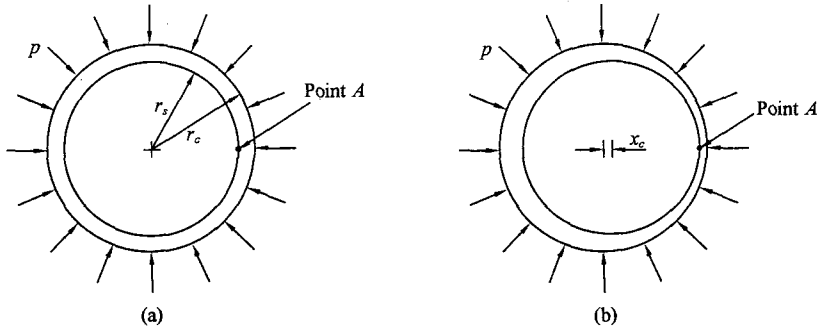


Fig. 4 Cross section of a shaft with coatings of (a) uniform and (b) non-uniform thickness.

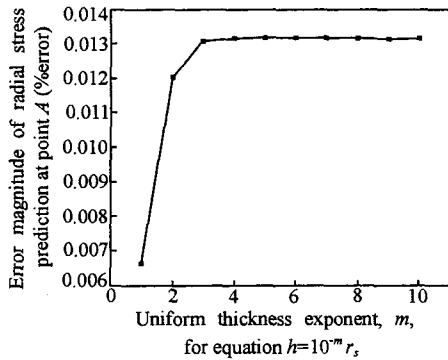


Fig. 5 Error magnitude of radial stress at point A for uniform coating thickness.

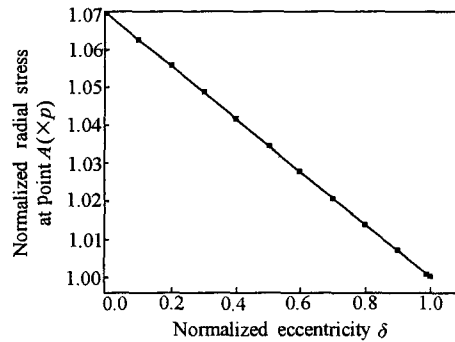


Fig. 6 Normalized radial stress at point A for nonuniform coating thickness.

approaches the applied pressure p as $\delta \rightarrow 1$, which is consistent with the physical interpretation. The results in Fig. 6 are almost the same as those in Ref. [3]. Very interesting comparison about the results and the number of nodes used between BEM and FEM can be seen in Ref. [3] as well.

From the above test examples, it can be seen that the present RHBNM is as suitable for thin structure problems as the BEM developed by Liu et al. [2,3].

V . DISCUSSION AND CONCLUSIONS

The applicability of the RHBNM for the analysis of thin shell-like structures is verified in this paper. It is shown that the present RHBNM, like the BEM developed by Liu et al. [2,3], can solve thin shell-like structures with very high accuracy by using a small number of nodes on the boundary. Instead of identifying the parts of a structure as plates, shells or solids, this approach can treat the structure as a single elastic medium and model it continuously without the need to shift to different models. The FEM modeling and analysis of shell-like structures are very delicate and demanding in engineering practices. However, it is very difficult, and sometimes even impractical, to distinguish among the thin shell, thick shell and solid models and then to choose the proper finite element types accordingly. The RHBNM developed may provide a very attractive numerical tool for the analysis of thin shell-like structures.

The RHBNM may be more appealing than the BEM developed by Liu et al [2,3] for its meshless

nature. It only requires randomly scattered nodal points to be constructed on the bounding surface of a body. Without meshing, it can directly use a solid model for a 3-D object. Therefore, it can be inter-linked with CAD software very easily.

By coupling with the Fast Multipole Method^[13], the RHBNM may be capable of solving large complicated structures. So it has very good prospects for application in practical engineering and is worth further investigation.

REFERENCES

- [1] Wang, X.C. and Shao, M., Basic principles and numerical processes of finite element method, Tsinghua University Press, Beijing, 1997 (in Chinese).
- [2] Liu, Y.J., Analysis of shell-like structures by the boundary element method based on 3-D elasticity: formulation and verification, *International Journal for Numerical methods in Engineering*, Vol.41, 1998, 541 – 558.
- [3] Luo, J.F., Liu, Y.J. and Berger, E.J., Analysis of two-dimensional thin structures (from micro- to nano-scales) using the boundary element method, *Computational Mechanics*, Vol.22, 1998, 404 – 412.
- [4] Belytchko, T., Lu, Y.Y. and Gu, L., Element free Galerkin methods, *International Journal for Numerical Methods in Engineering*, Vol.37, 1994, 229 – 256.
- [5] Zhu, T., Zhang, J. and Atluri, S.N., A local boundary integral equation (LBIE) method in computation mechanics, and a meshless discretization approach, *Computational Mechanics*, Vol.21, 1998, 223 – 235.
- [6] Atluri, S.N. and Zhu, T., A new meshless local Petrov-Galerkin approach in computational mechanics, *Computational Mechanics*, Vol.22, 1998, 117 – 127.
- [7] Mukherjee, Y.X. and Mukherjee, S., The boundary node method for potential problems, *International Journal for Numerical Methods in Engineering*, Vol.40, 1997, 797 – 815.
- [8] Zhang, J.M., Yao, Z.H. and Li, H., A hybrid boundary node method, *International Journal for Numerical Methods in Engineering*, Vol.53, 2002, 751 – 763.
- [9] Zhang, J.M. and Yao, Z.H., A new meshless regular hybrid boundary node method, *Computer Modeling in Engineering & Sciences*, Vol.2, 2001, 307 – 318.
- [10] Zhang, J.M. and Yao, Z.H., A new hybrid boundary node method for two-dimensional potential problem, *Journal of Chongqing Jianzhu University*, Vol.22, 2000, 103 – 107.
- [11] Belytchko, T., Krongauz, Y., Organ, D., Fleming, M. and Krysl, P., Meshless methods: an overview and recent developments, *Computer Methods in Applied Mechanics and Engineering*, Vol.139, 1996, 3 – 47.
- [12] DeFigueredo, T.G.B. and Brebbia, C.A., A new hybrid displacement variational formulation of BEM for elastostatics, Brebbia, C.A. and Conner, J.J. (eds.), *Advances in Boundary Elements*, Computational Mechanics Publications, Southampton, Vol.1, 1989, 47 – 57.
- [13] Popov, V. and Power, H., An $O(N)$ Taylor series multipole boundary element method for three-dimensional elasticity problems, *Engineering Analysis with Boundary Elements*, Vol.25, 2001, 7 – 18.